Europace (2007) **9**, vi38–vi45
doi:10.1093/europace/eum206

Influence of diffuse fibrosis on wave propagation in human ventricular tissue

Kirsten H.W.J. Ten Tusscher* and Alexander V. Panfilov

Department of Theoretical Biology, Utrecht University, Padualaan 8, 3584 CH Utrecht, The Netherlands

KEYWORDS
Fibrosis;
Arrhythmogenesis;
Re-entrant arrhythmias;
Spiral wave stability

Aims During ageing, after infarction, in cardiomyopathies and other cardiac diseases, the percentage of fibrotic (connective) tissue may increase from 6% up to 10–35%. The presence of increased amounts of connective tissue is strongly correlated with the occurrence of arrhythmias and sudden cardiac death.
Methods and results In this article, we investigate the role of diffuse fibrosis on wave propagation, arrhythmogenesis, and arrhythmia mechanism in human ventricular tissue using computer modelling. We show that diffuse fibrosis slows down wave propagation and increases tissue vulnerability to wave break and spiral wave formation. We also demonstrate that diffuse fibrosis increases the period of re-entrant arrhythmias and can suppress the restitution-induced transition from tachycardia to fibrillation.
Conclusion The latter suggests that mechanisms different from restitution-induced spiral break-up might be more likely to account for the onset of fibrillation in the presence of large amounts of diffuse fibrotic tissue.

Introduction

In the normal healthy heart, ~6% of the cardiac volume is made up of extracellular matrix (ECM) materials.[1] Non-excitable cardiac cells called fibroblasts produce the materials for the collagen and elastin fibrils making up the ECM. The ECM serves to anchor the cardiac muscle cells, determining cardiac structure,[1,2] thus playing an important role in cardiac mechanics and electrical impulse propagation.

During ageing and in various cardiac diseases, a remodelling of cardiac structure occurs, involving among other changes a substantial increase in the amount of ECM present in the heart. This process, which leads to fibrosis, is caused by the proliferation of fibroblasts and the subsequent disproportional deposition of interstitial collagens.[3,4] As a result of fibrosis formation, the percentage of connective tissue in the heart may increase up to 10–35%.[1] Fibrosis formation occurs after myocardial infarction, not just in the affected area to repair the infarct, but also in remote areas. In addition, it occurs in congestive heart failure, in a wide range of different cardiomyopathies (hypertensive, diabetic, ischaemic, dilated) and in diseases such as autoimmune myocarditis, Chagas' disease, and cardiac amyloidosis. Recently, it has become clear that in arrhythmogenic diseases that were previously mainly attributed to single ion channel mutations (for example Brugada syndrome), cardiac structural remodelling and fibrosis formation also occur.[5–7]

It is well known that increased amounts of fibrotic tissue in the heart are strongly correlated with an increased incidence of atrial and ventricular tachyarrhythmias and sudden cardiac death.[8–16] The exact mechanisms of arrhythmogenecity are not known, but it is widely believed that impaired electrical conduction plays an important role. Indeed, increased amounts of fibrosis have been found to lead to partial decoupling of muscle fibres, conduction slowing, zig-zag courses of conduction propagation, localized source–sink mismatches, and conduction blocks.[4,17] Clinical studies furthermore suggest that it is not just the amount, but also the architecture of the fibrosis that is important for its arrhythmogenecity.[17] In general, fibrotic tissue can occur in different forms: as diffuse randomly distributed small patches or as long string-like localized collagen depositions.[4,17] Stringy fibrosis causes more disruption of wave propagation than diffuse fibrosis and is considered to be more arrhythmogenic. However, large fibrotic strands can anchor spiral waves and thus stabilize the arrhythmia.[3]

Over the last decades, computer modelling has played an increasingly important role in cardiac arrhythmia research. However, despite the importance of fibrosis in arrhythmogenesis, most computer simulation research into tachyarrhythmias has so far focused on structurally normal cardiac tissue and only a few articles have dealt with modelling fibrotic tissue. Pertsov[18] studied the effects of large numbers of inexcitable obstacles mimicking fibrotic strands on wave propagation in a simplified model for cardiac tissue. He showed that textures of fibrotic strands may induce anisotropic propagation, widening and fractionation of electrograms, and influence the rotation of scroll waves. Recently, Turner *et al.*[19] showed that textures of string-like fibrotic obstacles lead to electrogram fractionation in human ventricular tissue simulated with the Priebe–Beuckelmann model. Spach *et al.*[20] simulated diffuse fibrosis by removing lateral

* Corresponding author. Tel: +31 30 2533695; fax: +31 30 2513655.
E-mail address: khwjtuss@hotmail.com

gap junctions in human atrial tissue modelled by the Nygren model. Increased heterogeneity in intercellular coupling was found to lead to vulnerability for partial wave block and re-entry. Kuijpers *et al*.[21] found that in human atrial tissue modelled by the Courtemanche model, heterogeneous uncoupling to model diffuse fibrosis leads to increased success of defibrillation shocks. Although these studies demonstrated that fibrosis could lead to increased vulnerability for re-entry, none of them investigated the influence of fibrosis on subsequent arrhythmia dynamics and stability.

In three previous articles,[22–24] we studied the possible effects of diffuse fibrosis on wave propagation, spiral wave dynamics, and spiral break-up-induced onset of fibrillatory excitation in cardiac tissue. We found that diffuse fibrosis increases the vulnerability of tissue to wave break and spiral wave formation, increases spiral wave rotation period and suppresses steep restitution-mediated spiral break-up. However, we used a simplified two variable FitzHugh–Nagumo model to simulate cardiac tissue.[22–24] Although these models can correctly describe the qualitative features of wave propagation in cardiac tissue, they do not reproduce quantitative relations of wave front width, action potential duration (APD), and size of fibrotic tissue patches, which have been shown to be important for wave propagation in fibrotic tissue.[18] In this article, we investigate the influence of diffuse fibrotic tissue on electrical conductance, vulnerability to arrhythmia occurrence, spiral and scroll wave dynamics, and steep restitution-mediated spiral break-up using a detailed ionic model for human ventricular tissue.[25,26]

Methods

Electrophysiological model

Ignoring the discrete character of microscopic cardiac cell structure, cardiac tissue can be modelled as a continuous system using the following partial differential equation:[27]

$$C_m \frac{\partial V_m}{\partial t} = \frac{\partial}{\partial x_i} D_{ij} \frac{\partial}{\partial x_j} V_m - I_{ion} \tag{1}$$

$$I_{ion} = I_{Na} + I_{to} + I_{CaL} + I_{Kr} + I_{Ks} + I_{K1} + I_{NaCa} + I_{NaK} + I_{pCa} + I_{pK} + I_{Na,b} + I_{Ca,b} \tag{2}$$

where C_m is the cellular capacitance, I_{ion} the sum of ionic transmembrane currents, and D_{ij} the diffusion tensor. To represent the electrophysiological properties specific for human ventricular tissue, we use our detailed ionic model for human ventricular myocytes that is based on a large range of human electrophysiological data.[25,26]

We used several parameter settings of our human ventricular cell model described in detail in Table 2 of Ten Tusscher and Panfilov.[26] To study the effect of diffuse fibrosis on the velocity of wave front propagation, commonly referred to as conduction velocity (CV), and vulnerability, we used the default parameter setting ('slope 1.1' from Table 2) of our model. To study the effect of fibrosis on the period of spiral wave rotation, we used an alternative parameter setting of our model with a shallow APD restitution curve ('slope 0.7' from Table 2), thus ensuring stable spiral wave rotation. To study the effect of diffuse fibrosis on steep APD restitution-mediated spiral break-up, we use a parameter setting with an APD restitution slope exceeding one ('slope 1.8' from Table 2), thus ensuring spiral break-up under non-fibrotic conditions.

Tissue geometry and diffusion tensor

Two-dimensional tissue geometry

In 2D, we used tissue sizes of 100 × 100 grid points to study conduction velocity (CV), tissue sizes of 100 × 100 to study vulnerability, tissue sizes of 320 × 320 to study stable spiral wave rotation, and tissue sizes of 800 × 800 to study spiral break-up. To simulate isotropic 2D tissue, we used for $D_{ij,}$ a tensor with 1.54 cm^2/s on the diagonals and 0 on the off-diagonal positions. The value of 1.54 cm^2/s ensures a plane wave conduction velocity of 70 cm/s, consistent with clinical measurements.[28]

Three-dimensional tissue geometry

In 3D, we used tissue sizes of 100 × 100 × 40 to study CV, tissue sizes of 100 × 100 × 40 to study vulnerability, tissue sizes of 320 × 320 × 40 to study stable spiral wave rotation, and tissue sizes of 600 × 600 × 28 to study spiral break-up. For 3D simulations, we used two different diffusion tensors: (i) D_{ij} with 1.54 cm^2/s on the diagonals and 0 on the off-diagonal positions to simulate fully isotropic tissue and (ii) D_{ij} the same as under (i), except for $D_{33} = 0.385$ cm^2/s to account for less strong coupling in the transmural direction. Unless explicitly stated differently, we used the second diffusion tensor for our 3D tissue simulations.

Human ventricular geometry

A 3D voxel description of human ventricular anatomy was obtained from an excised, structurally normal heart. The heart was positioned as in the thorax and digitized into 0.5 mm 3D voxels. The ventricular model consisted of a total of around 1.7 million grid points.

Action potential propagation occurs faster in the direction parallel to the muscle fibres, than in the direction perpendicular to the muscle fibres. To take the influence of muscle fibre direction into account in our ventricular model, a description of the myocardial fibre direction field is included. The local conductivity tensor D_{ij} is derived from the local fibre direction. Assuming that transverse conductivity is the same in all directions orthogonal to the direction of the muscle fibre axis, we described the ventricular conductivity tensor using the following equation:

$$D_{ij} = D_L \delta_{ij} + (D_L - D_T)\alpha_i \alpha_j \tag{3}$$

where α is the vector describing muscle fibre direction, and D_L and D_T are the conductivities in the longitudinal and transverse fibre directions, respectively. We use a ratio of 4:1 for D_L:D_T, which is within the range of experimentally recorded ratios.[28] $D_L = 1.54$ cm^2/s, the same as used above in 2D and 3D tissue.

Numerical integration

In the 2D simulations, we use simple forward Euler integration with a space step of 0.025 cm and a time step of 0.02 ms to integrate Eq. 1. The Rush and Larsen integration scheme[29] was used to integrate the Hodgkin–Huxley type equations for the gating variables of the various time-dependent currents (m, h, and j for I_{Na}, r and s for I_{to}, xr1 and xr2 for I_{Kr}, xs for I_{Ks}, d, f, f2, and fcass for I_{CaL}).

In the 3D and whole heart simulations, we use the method of operator splitting and adaptive time stepping to increase computational efficiency. Depending on the time derivative of the fast changing voltage and subspace calcium concentration variables, either a large time step ($t = 0.08$ ms) or a small time step ($t = 0.02$ ms) was used for integrating the reaction part of Eq. (1).

If the small time step was used, the integration was iterated four times. The diffusion part of Eq. (1) was always integrated with the large time step to ensure spatial synchronism of integration. In 3D tissue slabs, a space step of either 0.25 or 0.33 mm was used. In the ventricular simulations, a space step of 0.5 mm was used.

In all simulations, no-flux boundary conditions were imposed on the intracellular domain.

Fibrosis

Diffuse fibrosis in cardiac tissue was modelled by the presence of inexcitable obstacles of size 1×1 grid points in 2D or $1 \times 1 \times 1$ grid points in 3D that were randomly distributed across the tissue. The obstacles had no-flux boundaries. To investigate the influence of increasing amounts of diffuse fibrotic tissue during ageing or during a progressive disease process, different percentages of fibrotic obstacles replacing normal excitable cells were used.

Spiral waves

Spiral waves were initiated using a S1–S2 stimulus protocol, with the S2 stimulus applied in the refractory tail of the S1 wave, leading to partial propagation block and spiral wave formation. Stimulus currents were applied at twice the diastolic threshold.

Implementation

Two-dimensional simulations were coded in C++ and run on a single processor of a Dell 650 Precision Workstation (dual Intel xeon 2.66 GHz). Three-dimensional and ventricular simulations were coded in C++ and MPI and were run on 16 processors of a Beowulf cluster consisting of 14 Dell 650 Precision Workstations (dual Intel xeon 2.66 GHz).

Results

Planar conduction velocity

In the first set of computations, we investigate the influence of diffuse fibrosis on plane wave propagation in 2D tissue sheets and 3D tissue slabs. In 3D tissue, we investigated two different cases. In the first case, electrical coupling is the same in all three directions in the tissue. In the second case, electrical coupling in the *z*-direction is a factor 0.25 smaller than the electrical coupling in the *x,y* plane, which more closely resembles the situation in the ventricular wall.

Figure 1*A* and *B* shows snapshots of a planar wavefront progressing in small 2D planes of cardiac tissue with no fibrotic tissue and 30% of diffuse fibrotic tissue, respectively. Waves were initiated at the lower border of the tissues and snapshots were taken at the same time instant. We can see that the presence of fibrotic tissue delays wave propagation and leads to local disturbances in the wavefront. Figure 1*C* shows the planar CV as a function of the percentage fibrotic tissue present for 2D tissue, and the two different cases of 3D tissue. We can see that in 2D, CV decreases approximately linearly for up to 25% fibrosis, then decrease becomes steeper, and for more than 40% of fibrotic tissue propagation block occurs. We can see that in 3D for moderate (up to 25%) fibrosis, the CV decreases in a fashion similar to 2D tissue. For more than 25% fibrosis, the CV in 3D decreases less strongly than in 2D. In 3D tissue, propagation block occurs for more than 65% fibrosis, compared with 40% in 2D tissue. In addition, we can see that CV decrease is slightly stronger for the 3D case with lower electrical coupling in the *z*-direction.

Overall, we see that 3D propagation is less hampered by diffuse fibrosis, which can be explained by the fact that the third dimension offers an alternative route for the excitation wave.

Vulnerability

In cardiac tissue with anatomical or functional heterogeneities, re-entrant sources (spiral waves) can be initiated by the application of two stimuli at the same location, if the coupling time between the two stimuli is within some time interval, called the vulnerable period or window.[30–34] Here, we tested whether diffuse fibrosis—large numbers of small inexcitable obstacles—can induce wave break and spiral wave formation in human ventricular tissue. Note that in this case the characteristic wavelength of the excitation wave (1–3 cm) is an order of magnitude larger than the spatial scale of the heterogeneities (0.25 mm). We found that for substantial percentages of fibrotic tissue two closely timed stimuli could lead to wave break and spiral wave formation.

Figure 2A shows the snapshots of two waves with a short coupling interval (321 ms) between them applied in a 2D medium with 10% fibrotic tissue. We can see that the second wave is blocked at some locations; however, the breaks are repaired when the wavefront proceeds, thus not leading to the formation of spiral waves. *Figure 2B* shows similar snapshots in a medium with 30% fibrosis (coupling interval 320 ms). Now the second wavefront is blocked in larger regions, causing not all breaks to be repaired and spiral wave formation to occur.

We determined the size of the vulnerable window in 2D tissue sheets, 3D tissue slabs, and the human ventricular geometry. In 2D and 3D tissue, we applied two subsequent stimuli to a border of the tissue sheet or slab. In the ventricles, we applied two subsequent stimuli to the endocardial surface of the ventricles, to mimic the normal endocardial to epicardial ventricular activation sequence. *Figure 3* plots the width of the vulnerable window as a function of the percentage of diffuse fibrosis. The vulnerable window

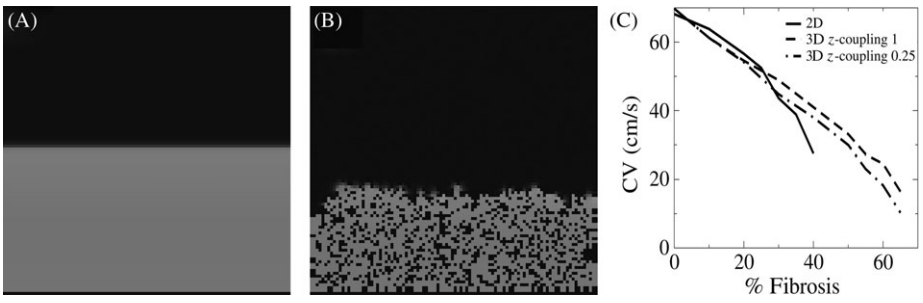

Figure 1 Conduction slowing by diffuse fibrosis. (*A*) Plane wave propagation in 2D tissue without fibrotic tissue. (*B*) Plane wave propagation in 2D tissue with 30% fibrosis. (*C*) Planar conduction velocity as a function of the percentage fibrosis in 2D tissue, 3D tissue with equal coupling in all three directions (*z*-coupling 1), and 3D tissue with weaker coupling in the third dimension (*z*-coupling 0.25).

is defined here as the coupling intervals between two stimuli that lead to wave breaks and subsequent spiral wave formation. We see that in 2D tissue (*Figure 3A*), for $<$10% fibrosis no vulnerable window is present and either normal propagation or full propagation block occurs. For more than 10% fibrosis, a vulnerable window appears and its width increases with the percentage of fibrosis. In 3D tissue slabs (*Figure 3B*), a vulnerable window is present for more than 20% fibrosis, and its width is considerably smaller than in 2D tissue. In the ventricular geometry (*Figure 3C*), a vulnerable window is present for more than 10% fibrosis and its width is somewhere between that of the window found in 2D and 3D tissue.

Spiral wave rotation

Ventricular tachycardia and fibrillation are thought to be caused by re-entrant (spiral) waves of excitation.[35–40] Therefore, we investigate the influence of diffuse fibrotic tissue on spiral wave dynamics.

Figure 4 shows the stable spiral wave rotation in 2D tissue sheets for 0, 10, and 30% fibrosis, in 3D tissue slabs for 0, 30, and 60% fibrosis, and in the ventricles for 0, 30, and 50% fibrosis. We can see that in all cases rotation of the spiral wave remains stable and no wave breaks or turbulence occurs. However, an increase in the percentage of fibrosis leads to a less regular wavefront pattern and some shortening of the wavelength (excited region).

To investigate more quantitatively the effect of diffuse fibrosis on spiral wave dynamics, we measured period, diastolic interval (DI), and APD during spiral wave rotation as a function of the percentage diffuse fibrosis. *Figure 5* shows the results for the spiral wave period. In 2D (solid line), we can see a gradual increase in spiral wave period for up to 30–35% of fibrosis and a much stronger period increase for higher percentages of fibrosis. In 3D (dashed line), the stronger increase in period starts at $\sim$50% fibrosis. In the ventricular geometry (dotted-dashed line), the dependence of spiral wave period on fibrosis percentage lies between that in 2D and 3D tissue.

It has been shown in 3D tissue modelled with FitzHugh–Nagumo type models that when a 3D scroll wave is extended along regions with different properties, the overall scroll wave period is determined by wave rotation in the most excitable region.[24,41,42] In 3D fibrotic tissue, the percentage of fibrosis is assigned to the entire tissue slab, not to individual layers. As a consequence, the different tissue layers not only have a different random pattern of inexcitable obstacles, but also have a somewhat different percentage of fibrosis. These differences allow the individual layers to support spiral waves with different periods of rotation. We therefore hypothesize that the mechanism of a fast layer driving the complete 3D tissue slab explains the different dependence of spiral period on fibrosis in 2D vs. 3D tissue. To test this hypothesis, we compared the two following simulations: in one simulation, we computed spiral wave rotation periods in a 3D tissue slab with 35% fibrotic tissue in which we decoupled the horizontal layers from each other. We compared the resulting independent spiral periods with the scroll wave period in a fully coupled simulation of the same 3D tissue slab.

Figure 6 plots the spiral period as a function of layer in the 3D (decoupled) tissue. We can see that each layer has its own independent spiral wave period, with a maximum period of 281 ms in layer 25, a minimum period of 236 ms in layer 5, and a mean period of 259 ms. For comparison, we also show scroll wave period in the coupled 3D tissue, which is the same in all layers of the tissue and is 234 ms. Note that scroll wave period in the coupled tissue indeed is approximately equal to the shortest spiral wave period found in the uncoupled simulation, supporting our hypothesis.

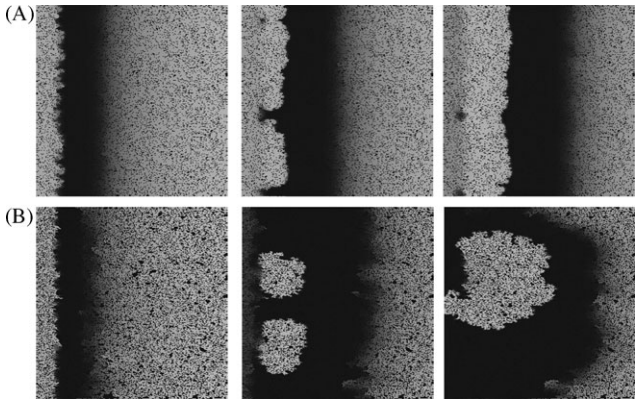

Figure 2 Vulnerability to wave break and spiral wave formation due to diffuse fibrosis. (*A*) Snapshots of progression of two wavefronts initiated in a medium with 10% fibrosis and with a coupling interval of 321 ms between them. (*B*) Snapshots of progression of two wavefronts initiated in a medium with 30% fibrosis and with a coupling interval of 320 ms between them.

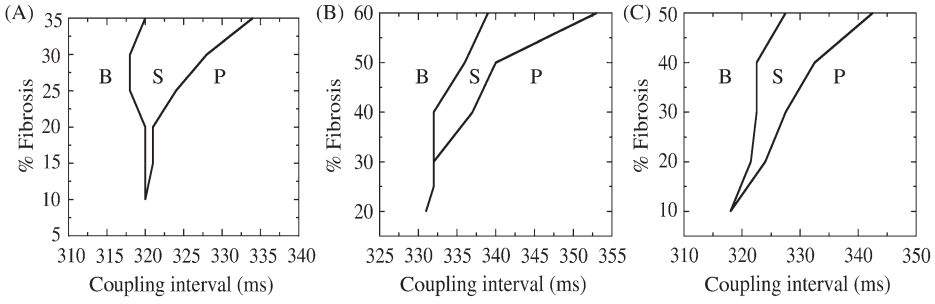

Figure 3 Vulnerable window as a function of the percentage fibrosis. Vulnerability is determined by applying two stimuli at the same location with different coupling intervals between them. B, full block of propagation of the second wavefront; P, full propagation of the second wavefront; S, the occurrence of wave break and spiral wave formation. Vulnerable window in (*A*) 2D tissue sheets, (*B*) 3D tissue slabs, and (*C*) human ventricular geometry.

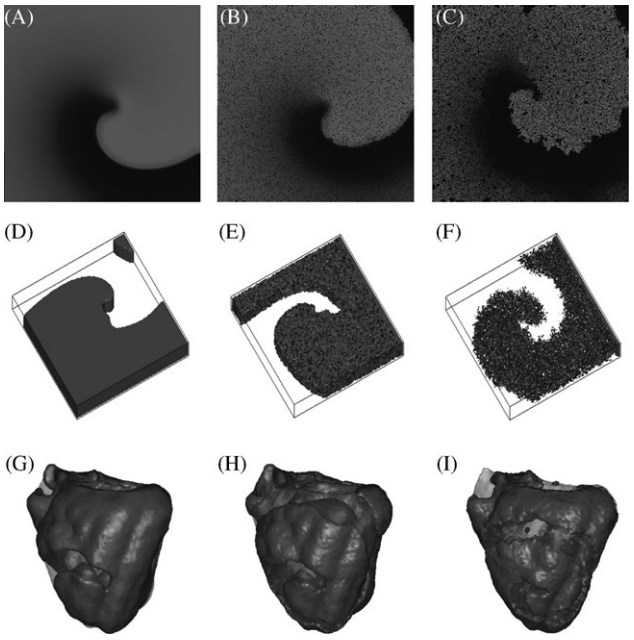

Figure 4 Stable spiral wave rotation in 2D tissue sheets with (*A*) 0, (*B*) 10, and (*C*) 30% fibrosis. Spiral rotation in 3D tissue slabs with (*D*) 0, (*E*) 30, and (*F*) 60% fibrosis, and in the human ventricular geometry with (*G*) 0, (*H*) 30, and (*I*) 50% fibrosis.

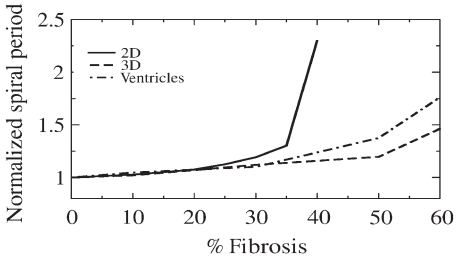

Figure 5 Spiral period increase due to diffuse fibrosis. Period of spiral wave rotation as a function of the percentage fibrosis in 2D tissue, 3D tissue, and the ventricular geometry. Spiral wave periods are normalized relative to the spiral wave period in tissue without fibrosis.

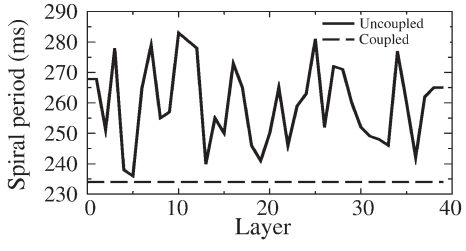

Figure 6 Spiral rotation period in 3D tissue slabs with 35% fibrosis as a function of tissue layer for a slab in which the layers are uncoupled (solid line) and a slab in which the layers are coupled (dashed line).

Spiral break-up

One frequently discussed hypothesis for ventricular fibrillation is the so-called restitution hypothesis. According to this hypothesis the onset of turbulent wave patterns is the result of the break-up of spiral waves. This break-up occurs in cardiac tissue with a steep APD restitution curve, which leads to action potential alternans instability.[43–46] Here we investigated the influence of diffuse fibrotic tissue on the occurrence of steep APD restitution-induced spiral break-up.

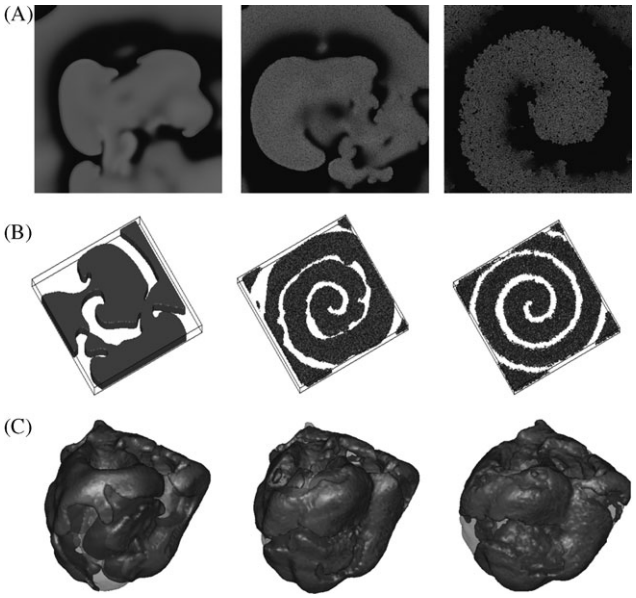

Figure 7 Suppression of spiral break-up by diffuse fibrosis. (*A*) Spiral dynamics for spiral break-up parameter settings in 2D tissue with 0, 10, and 35% fibrosis, (*B*) in 3D tissue with 0, 40, and 50% fibrosis, and (*C*) in the ventricles with 0, 30, and 40% fibrosis.

Figure 7A shows a series of snapshots of spiral dynamics in 2D tissue with no fibrosis, 10 and 35% fibrosis present, respectively. We can see that for 0% fibrosis spiral break-up occurs and subsequent fibrillation-like dynamics develop. The presence of 10% fibrosis causes the break-up pattern to be less chaotic, and 35% fibrosis completely suppresses spiral break-up.

In *Figure 7B,* we show similar simulations in 3D tissue, but with fibrosis percentages of 0, 40, and 50%, respectively. For 0% fibrosis, spiral break-up develops. For 40% fibrosis, wave break formation starts to develop towards the end of the simulation, indicating that break-up is delayed but not fully suppressed. Note that for this percentage of fibrosis, break-up is fully suppressed in 2D tissue. For 50% fibrosis, break-up is completely suppressed. Thus, in both 2D and 3D tissue, diffuse fibrosis can fully suppress spiral break-up; however, in 3D tissue a percentage of 50% or more fibrosis is required, whereas in 2D tissue the presence of 30–35% fibrotic tissue is sufficient to suppress break-up.

Figure 7C shows the spiral wave dynamics in the ventricles for 0, 30, and 40% fibrosis. For 0% fibrosis, spiral break-up and fibrillatory-like wave patterns develop. For 30% fibrosis, no full-blown fibrillatory patterns develop but wave breaks and wave pattern disorganization do occur. For 40% fibrosis, wave break and spiral break-up are fully suppressed. Thus, the percentage of diffuse fibrosis fully suppressing spiral break-up in the ventricular geometry lies between the percentages found in 2D and 3D tissue.

In *Figure 8*, we explain the mechanism of break-up suppression by diffuse fibrosis. In our model, spiral break-up

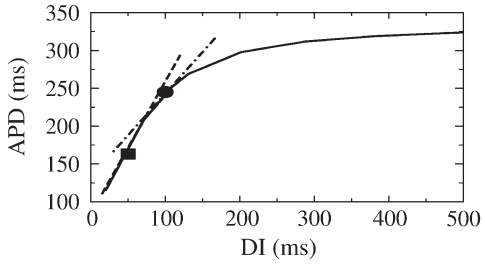

Figure 8 Restitution curve showing the dependence of action potential duration (APD) on diastolic interval (DI) for the parameter setting used in *Figure 7*. The restitution curve was obtained using a dynamic restitution protocol. The square indicates the APD, DI pair corresponding to spiral wave rotation in 2D tissue with no fibrosis, the circle indicates the APD, DI values corresponding to spiral wave rotation in 2D tissue with 35% fibrotic tissue.

occurs as a result of dynamical instabilities in APD due to steep APD restitution. Because of the shape of the restitution curve, the slope of the restitution curve decreases if the DI and APD increase (*Figure 8*). In general, fibrosis increases the period, APD and DI of spiral wave rotation (*Figure 5*). As a consequence, the slope of the part of the restitution curve visited during spiral wave rotation becomes less steep. This is illustrated in *Figure 7*, where the square indicates the DI during spiral wave rotation in 2D tissue without fibrosis, and the circle indicates the DI for spiral wave rotation in 2D tissue with 35% fibrosis. We clearly see a decrease in the slope of the part of the restitution curve that is visited, which explains the stabilization of spiral wave rotation in *Figure 7A3*.

The difference in percentage of fibrosis needed to suppress break-up in 2D and 3D tissue can be explained as follows: we found (*Figure 5*) that for similar percentages of fibrosis, spiral wave period increases more in 2D than in 3D. As a consequence, to suppress spiral break-up by shifting the system along the restitution curve due to a period increase, a much larger percentage of obstacles is needed in 3D than in 2D.

Discussion

Ventricular tachycardia and fibrillation predominantly occur in aged and diseased hearts, where cardiac remodelling among other changes has led to fibrosis, the increased deposition of ECM materials. The increase in interstitial collagen influences both the mechanical and the electrical function of the heart, increasing muscle stiffness and reducing coupling between adjacent muscle fibre bundles.

Clinical studies have suggested a role for fibrotic tissue in wave break and phase singularity formation,[47] conduction delays, conduction blocks, and zig-zag course of conduction.[4,17] Clinical studies furthermore suggest that apart from the amount, it is especially the pattern of fibrosis, diffuse or stringy, that plays an important role in arrhythmogenecity.[17] However, how precisely fibrosis leads to arrhythmia generation and maintenance remains unclear.

In this article, we investigated the influence of diffuse fibrosis on wave propagation, vulnerability to wave break and spiral wave formation and on steep APD restitution-mediated spiral break-up in human ventricular tissue, using the method of computer modelling. We modelled diffuse fibrosis by the presence of small sized, randomly distributed inexcitable obstacles in the tissue. In previous studies, using FitzHugh–Nagumo type models to describe cardiac tissue, we found that small-sized obstacles could have a significant effect on wave propagation, vulnerability, and spiral dynamics.[23,24] However, in FitzHugh–Nagumo type models, the upstroke of the action potential is slow and the wavelength is short compared with human ventricular action potential dynamics and duration. This may influence the amount of effect that small obstacles have on wave propagation.[18] Therefore, in the current study we used an electrophysiologically detailed model for human ventricular cells, previously developed by our group,[25,26] to specifically model human ventricular tissue with diffuse fibrosis.

We found that despite the small size of the obstacles (length 0.25–0.5 mm) relative to the wavelength in human ventricular tissue (1–3 cm), the presence of diffuse fibrosis has significant effects on wave propagation. We showed that planar wave CV decreases more or less linearly with percentage of fibrosis. However, in 2D, above 25% CV starts to decrease faster as fibrosis increases, and for more than 40% fibrosis conduction block occurs, whereas in 3D conduction proceeds up to 65% fibrosis. We also found that diffuse fibrosis leads to the presence of a vulnerable window during which wave break and spiral wave formations occur. This vulnerable window is larger in 2D than in 3D tissue, due to the alternative routes offered by the third dimension to restore wave breaks in adjacent layers.

We showed that fibrosis leads to an increase in spiral wave rotation period both in 2D and 3D tissue, with the effect in 2D being more pronounced, and explained the mechanism behind this difference. On the basis of these results we expect that the average period of cardiac arrhythmias increases with increasing amounts of diffuse fibrosis. It would be interesting to check this prediction against available clinical data.

Finally, we showed that the presence of diffuse fibrosis suppresses spiral break-up caused by steep APD restitution: diffuse fibrosis slows down spiral wave rotation and thus increases DI, shifting the system to a more shallow part of the APD restitution curve, which suppresses spiral break-up. Again, this effect is stronger in 2D than in 3D tissue. In 3D tissue, spiral period increases less with the percentage of fibrosis. As a consequence, the shift along the restitution curve and break-up suppressing effect induced by fibrosis in 3D will also be less.

It is important to note here that steep restitution spiral break-up is only one of the possible mechanisms for ventricular fibrillation. Examples of other mechanisms are 3D (rotational anisotropy,[48] transmural refractoriness gradient,[49] and negative filament tension[50]) spiral break-up, triggered activity (EADs, DADs[51–53]), abnormal automaticity, and fibrillatory conduction.[54,55] One or more of these other mechanisms may be enhanced by the presence of diffuse fibrotic tissue. For example, the spread of activation from a point where triggered activity or abnormal automaticity occurs is enhanced under conditions of decreased electrotonic loading, which occur due to increased fibrosis.[56]

Note that for all effects studied here, the influence of diffuse fibrosis on conduction is stronger in 2D than in 3D tissue, and the effect of fibrosis in the ventricular geometry is somewhere in between these two cases.

Qualitatively, the results of our current study are similar to our previous findings using FitzHugh–Nagumo type models.[23,24] Given the substantial differences between these models, this suggests that the reported effects of diffuse fibrosis on wave propagation and re-entry dynamics are general and can also be found in other models of cardiac tissue and real cardiac tissue. However, quantitatively, there are substantial differences. In the FitzHugh–Nagumo model, CV decreases more strongly as a function of percentage fibrosis (25% CV decrease for 20% fibrosis) than in our human ventricular tissue model (17% CV decrease for 20% fibrosis). Also, in the FitzHugh–Nagumo model, a vulnerable window is present for percentages of fibrosis just over 0%, whereas in our human ventricular tissue model in 2D 10%, in 3D 20%, and in the ventricles 10% fibrosis or more is needed to create a vulnerable window. Furthermore, the increase in spiral wave rotation period as a function of percentage of diffuse fibrosis is stronger in the FitzHugh–Nagumo model than in our human ventricular tissue model. As a consequence, higher percentages of diffuse fibrosis are required to suppress steep restitution break-up in our human ventricular tissue model. Overall, the influence of diffuse fibrosis is less strong in our detailed ionic human ventricular tissue model than in the simplified phenomenological FitzHugh–Nagumo model. These quantitative differences might be due to the smaller size of the obstacles relative to the wavelength in our human ventricular tissue model.

Limitations

There are some limitations to the current modelling study. A first limitation is that apart from the presence of fibrotic tissue, the ventricular tissue we simulated is homogeneous in terms of ionic properties. We did not include known differences between epicardial, endocardial, and mid-myocardial cells or other known ionic gradients. The partial uncoupling that is caused by the presence of fibrotic tissue reduces electrotonic coupling and may hence enhance ionic tissue heterogeneities, thus further enhancing vulnerability. A second limitation is that we only studied the influence of fibrotic tissue itself, and not the influence of concomitant changes in gap junctional coupling and ionic properties that also occur during tissue remodelling. These may further affect vulnerability and spiral wave dynamics.

A third limitation is that we only investigated the effect of diffuse fibrosis on one potential fibrillation mechanism, and did not study its effect on focal or fibrillatory conduction-driven fibrillation. A final limitation of our model is that we used a monodomain description for cardiac tissue, whereas for tissue with inexcitable fibrotic obstacles a bidomain description distinguishing intra and extracellular potentials may be more appropriate.

Conclusion

We show that the presence of diffuse fibrosis can explain the increased vulnerability to arrhythmias observed in patients with (diffuse) fibrosis. Our results suggest that diffuse fibrosis can suppress steep restitution spiral break-up by slowing down of re-entry, causing this to be a less likely mechanism for fibrillation in fibrotic hearts. On the basis of our results, we also expect that the effects of fibrotic tissue are more pronounced in thin (atrial) than in thick (ventricular) cardiac tissue.

Conflict of interest: none declared.

Funding

This work was supported by the Netherlands Organization for Scientific Research (NWO) through grant number 635100004 of the Research Council for Physical Sciences (EW) (KHWJTT).

References

1. Rossi MA. Connective tissue skeleton in the normal left ventricle and in hypertensive left ventricular hypertrophy and chronic chagasic myocarditis. *Med Sci Monit* 2001;**7**:820–32.
2. Jugdutt BI. Remodelling of the myocardium and potential targets in the collagen synthesis pathways. *Curr Drug Targets Cardiovasc Haematol Disord* 2003;**3**:1–30.
3. De Bakker JM, Stein M, Van Rijen HM. Three-dimensional anatomic structure as substrate for ventricular tachycardia/ventricular fibrillation. *Heart Rhythm* 2005;**2**:777–9.
4. De Bakker JM, Van Rijen HM. Continuous and discontinuous propagation in heart muscle. *J Cardiovasc Electrophysiol* 2006;**17**:567–73.
5. Meregalli PG, Wilde AA, Tan HL. Pathophysiological mechanisms of brugada syndrome: depolarization disorder, repolarization disorder, or more? *Cardiovasc Res* 2005;**67**:367–78.
6. Frustaci A, Priori SG, Pieroni M, Chimenti C, Napolitano C, Rivolta I *et al*. Cardiac histological substrate in patients with clinical phenotype of brugada syndrome. *Circulation* 2005;**13**:3680–7.
7. Coronel R, Casini S, Koopmann TT, Wilms-Schopman FJ, Verkerk AO, de Groot JR *et al*. Right ventricular fibrosis and conduction delay in a patient with clinical signs of brugada syndrome: a combined electrophysiological, genetic, histopathologic, and computational study. *Circulation* 2005;**112**:2769–77.
8. Everett TH, Olgin JE. Atrial fibrosis and the mechanisms of atrial fibrillation. *Heart Rhythm* 2007;**4**:S24–7.
9. Saito T, Tamura K, Uchida D, Saito T, Togashi M, Nitta T *et al*. Histopathological features of the resected left atrial appendage as predictors of recurrence after surgery for atrial fibrillation in valvular heart disease. *Circ J* 2007;**71**:70–8.
10. Nakai T, Chandy J, Nakai K, Bellows WH, Flachsbart K, Lee RJ *et al*. Histologic assessment of right atrial appendage myocardium in patients with atrial fibrillation after coronary artery bypass graft surgery. *Cardiology* 2006;**108**:90–6.
11. Strain JE, Grose RM, Factor SM, Fisher JD. Results of endomyocardial biopsy in patients with spontaneous ventricular tachycardia but without apparent structural heart disease. *Circulation* 1983;**68**:1171–81.
12. Segawa I, Suzuki T, Kato M, Tashiro A, Satodata R. Relation between myocardial histological changes and ventricular tachycardia in cardiomyopathy: a study by 24-hour ecgmonitoring and endomyocardial biopsy. *Heart Vessels* 1990;**Suppl 5**:37–40.
13. Assomull RG, Prasad SK, Lyne J, Smith G, Burman ED, Khan M *et al*. Cardiovascular magnetic resonance, fibrosis, and prognosis in dilated cardiomyopathy. *J Am Coll Cardiol* 2006;**48**:1977–85.
14. John BT, Tamarappoo BK, Titus JL, Edwards WD, Shen WK, Chugh SS. Global remodeling of the ventricular interstitium in idiopathic myocardial fibrosis and sudden cardiac death. *Heart Rhythm* 2004;**1**:141–9.
15. Hsia HH, Marchlinski FE. Characterization of the electroanatomic substrate for monomorphic ventricular tachycardia in patients with nonischemic cardiomyopathy. *Pacing Clin Electrophysiol* 2002;**25**:1114–27.
16. Varnava AM, Elliott PM, Mahon N, Davies MJ, McKenna WJ. Relation between myocyte disarray and outcome in hypertrophic cardiomyopathy. *Am J Cardiol* 2001;**88**:275–9.
17. Kawara T, Derksen R, De Groot JR, Coronel R, Tasseron S, Linnenbank AC *et al*. Activation delay after premature stimulation in chronically diseased human myocardium relates to the architecture of interstitial fibrosis. *Circulation* 2001;**104**:3069–75.
18. Pertsov A. Scale of geometric structures responsible for discontinuous propagation in myocardial tissue. In: Spooner P, Joyner RW, Jalife J. *Discontinuous Conduction in the Heart*. Armonk, NY: Futura Publishing Company; 1997.

19. Turner I, Huang C, Saumarez RC. Numerical simulation of paced electrogram fractionation: relating clinical observations to changes in fibrosis and action potential duration. *J Cardiovasc Electrophysiol* 2005;**16**: 151–61.
20. Spach MS, Heidlage JF, Dolber PC, Barr RC. Mechanism of origin of conduction disturbances in aging human atrial bundles: experimental and model study. *Heart Rhythm* 2007;**4**:175–85.
21. Kuijpers NH, Keldermann RH, Arts T, Hilbers P. Computer simulations of successful defibrillation in decoupled and non-uniform cardiac tissue. *Europace* 2005;**7**:166–77.
22. Panfilov AV. Spiral breakup in an array of coupled cells: the role of the intercellular conductance. *Phys Rev Lett* 2002;**88**:118101.
23. Ten Tusscher KHWJ, Panfilov AV. Influence of nonexcitable cells on spiral breakup in two-dimensional and three-dimensional excitable media. *Phys Rev E Stat Nonlin Soft Matter Phys* 2003;**68**:062902.
24. Ten Tusscher KHWJ, Panfilov AV. Wave propagation in excitable media with randomly distributed obstacles. *Multiscale Model Simul* 2005;**3**: 265–82.
25. Ten Tusscher KHWJ, Noble D, Noble PJ, Panfilov AV. A model for human ventricular tissue. *Am J Physiol Heart Circ Physiol* 2004;**286**:H1573–89.
26. Ten Tusscher KHWJ, Panfilov AV. Alternans and spiral breakup in a human ventricular tissue model. *Am J Physiol Heart Circ Physiol* 2006;**291**: H1088–100.
27. Keener J, Sneyd J. *Mathematical Physiology*. New York, Heidelberg, Berlin: Springer-Verlag; 1998.
28. Taggart P, Sutton PMI, Opthof T, Coronel R, Trimlett R, Pugsley W *et al*. Inhomogeneous transmural conduction during early ischemia in patients with coronary artery disease. *J Mol Cell Cardiol* 2000;**32**:621–39.
29. Rush S, Larsen H. A practical algorithm for solving dynamic membrane equations. *IEEE Trans Biomed Eng* 1978;**25**:389–92.
30. Krinsky VI. Spread of excitation in an inhomogeneous medium (state similar to cardiac fibrillation). *Biophysics* 1966;**11**:776–84.
31. Panfilov AV, Vasiev BN. Vortex initiation in a heterogeneous excitable medium. *Physica D* 1991;**49**:107–13.
32. Panfilov AV, Keener JP. Effects of high frequency stimulation on cardiac tissue with an inexcitable obstacle. *J Theor Biol* 1993;**163**:439–48.
33. Agladze KI, Keener JP, Muller SC, Panfilov AV. Rotating spiral waves created by geometry. *Science* 1994;**264**:1746–8.
34. Cabo C, Pertsov AM, Davidenko JM, Baxter WT, Gray RA, Jalife J. Vortex shedding as a precursor of turbulent electrical activity in cardiac muscle. *Biophys J* 1996;**70**:1105–11.
35. Allessie MA, Bonke FIM, Schopman GFJ. Circus movement in rabbit atrial muscle as a mechanism of tachycardia. *Circ Res* 1973;**33**:54–62.
36. Davidenko JM, Pertsov AM, Salomonsz R, Baxter W, Jalife J. Stationary and drifting spiral waves of excitation in isolated cardiac muscle. *Nature* 1992;**355**:349–51.
37. Gray RA, Jalife J, Panfilov AV, Baxter WT, Cabo C, Davidenko JM *et al*. Mechanisms of cardiac fibrillation. *Science* 1995;**270**:1222–3.
38. Winfree AT. Electrical instability in cardiac muscle: phase singularities and rotors. *J Theor Biol* 1989;**138**:353–405.
39. Winfree AT. Electrical turbulence in three-dimensional heart muscle. *Science* 1994;**266**:1003–6.
40. Jalife J, Gray R. Drifting vortices of electrical waves underlie ventricular fibrillation in the rabbit heart. *Acta Physiol Scand* 1996;**157**:123–31.
41. Panfilov AV. Three-dimensional vortices in active media. In: Holden AV, Markus M, Othmer HG. *Nonlinear Wave Processes in Excitable Media*. New York: Plenum Press; 1991. 361–82.
42. Panfilov AV, Keener JP. Twisted scroll waves in heterogeneous excitable media. *Int J Bif Chaos* 1993;**3**:445–50.
43. Nolasco J, Dahlen R. A graphic method for the study of alternation in cardiac action potentials. *J Appl Physiol* 1968;**25**:191–6.
44. Guevara M, Ward A, Shrier A, Glass L. Electrical alternans and period doubling bifurcations. *IEEE Comp Cardiol* 1984;**562**:167–70.
45. Panfilov AV, Hogeweg P. Spiral break-up in a modified FitzHugh–Nagumo model. *Phys Lett A* 1993;**176**:295–9.
46. Karma A. Spiral breakup in model equations of action potential propagation in cardiac tissue. *Phys Rev Lett* 1993;**71**:1103–6.
47. Wu TJ, Ong JJC, Hwang C, Lee JJ, Fishbein MC, Czer L *et al*. Characteristics of wave fronts during ventricular fibrillation in human hearts with dilated cardiomyopathy: role of increased fibrosis in the generation of reentry. *J Am Coll Cardiol* 1998;**32**:187–96.
48. Fenton F, Karma A. Vortex dynamics in three-dimensional continuous myocardium with fiber rotation: filament instability and fibrillation. *Chaos* 1998;**8**:20–47.
49. Mikhailov AS, Panfilov AV, Rudenko AN. Twisted scroll waves in active threedimensional media. *Phys Lett A* 1985;**109**:246–9.
50. Biktashev VN. A three-dimensional autowave turbulence. *Int J Bif Chaos* 1998;**8**:677–84.
51. Ashihara T, Yao T, Namba T, Kawase A, Ikeda T, Nakazawa K. Afterdepolarizations promote the transition from ventricular tachycardia to fibrillation in a three-dimensional model of cardiac tissue. *Circ J* 2002;**66**: 505–10.
52. Huffaker RB, Lamp ST, Weiss JN, Kogan B. Intracellular calcium cycling, early afterdepolarizations, and reentry in a simulated long qt syndrome. *Heart Rhythm* 2004;**1**:441–8.
53. Huffaker RB, Weiss JN, Kogan B. Effects of early afterdepolarizations on reentry in cardiac tissue: A simulation study. *Am J Physiol Heart Circ Physiol* 2007;**292**:H3089–102.
54. Jalife J. Ventricular fibrillation: mechanisms of initiation and maintenance. *Annu Rev Physiol* 2000;**62**:25–50.
55. Jalife J, Berenfeld O, Mansour M. Mother rotors and fibrillatory conduction: a mechanism of atrial fibrillation. *Cardiovasc Res* 2002;**54**:204–16.
56. Wilders R, Wagner MB, Golod DA, Kumar R, Wang Y, Goolsby WN *et al*. Effects of anisotropy on the development of cardiac arrhythmias associated with focal activity. *Pflugers Arch* 2000;**441**:301–12.